Inhibition Effect of 2,2'-bipyridyl on the Corrosion of Austenitic Stainless Steel in 0.5M H_2SO_4

AMEL GHARBI[1,2], ABDELAZIZ HIMOUR[1], SIHEM ABDERRAHMANE[1]* and KARIMA ABDERRAHIM[2]

[1]Surface Engineering Laboratory (L.I.S), Badji Mokhtar University, B.P.12-23000, Annaba, Algeria.
[2]Research Center In industrial Technology CRTI, P.O.Box 64, Cheraga 16014 Algiers, Algeria.
*Corresponding author E-mail: abderrahmanesihem@yahoo.fr

ABSTRACT

The corrosion inhibition of AISI309 austenitic stainless steel by 2,2'-Bipyridyl in 0.5M H_2SO_4 at 298K was studied using the mass loss' method, the potentiodynamic polarization (Tafel), the linear polarization (LRP) and the electrochemical impedance spectroscopy (EIS). The results showed a mixed inhibition mode and an increase in the charge transfer resistance, due to inhibitor molecules' adsorption at steel surface. This latter obeys to Langmuir isotherm. The observation by scanning electron microscopy (SEM) and the analysis by energy dispersion spectrometry (EDS) confirm an inhibitor film's presence. The calculated inhibition efficiencies are in accordance with 87.78% maximum value.

Keyword: AISI309, 2,2'-Bipyridyl, Corrosion; Inhibition, EIS, Tafel.

INTRODUCTION

Austenitic stainless steels are widely used as building materials in the following fields: medical, automotive, food[1], steam power stations[2], piping systems, chemical factories and heat exchanger equipment[3]. Their resistance to corrosion is due to passive film formation of chromium oxide on the surface. However, these steels are sensitive to corrosion in certain acidic media[4], including sulfuric acid and hydrochloric acid which are widely used for stripping, cleaning and descaling industrial processes[5,6].

The organic inhibitors' use is a practical, economical and effective method of protecting materials against corrosion[7]. The heterocyclic organic compounds containing Nitrogen are considered in the literature as mild steel's efficient corrosion inhibitors in acidic media[8]. Generally, the adsorption mechanism of these compounds is made by heteroatoms such as nitrogen, oxygen

and sulfur[9,10] and depends on inhibitor's physic-chemical properties, electrolyte's chemical composition and metal nature[11,12].

Among the heterocyclic organic compounds, pyridine and its derivatives are effective inhibitors against mild steels' corrosion in hydrochloric acid[13-20]. Moreover, pyridine plays a very important role in biological activity by its presence in natural and pharmaceutical products; generally, its derivatives possess various pharmacological properties[13,21]. However, few studies were carried out on pyridine and its derivatives as stainless steels' corrosion inhibitors in H_2SO_4[22, 23].

Organic compounds containing a single pyridine ring are the most used, whereas those containing several rings are rarely used, so it is necessary to study the steel inhibition by these compounds with pyridine several rings which efficiency is important.

In this work, the main objective is to study the corrosion inhibition of AISI309 austenitic stainless steel by 2,2'-Bipyridyl in 0.5M H_2SO_4, this inhibitor contains two pyridine rings. The corrosion behavior was pursued by the weight loss method, potentiodynamic polarization (Tafel), electrochemical impedance spectroscopy (EIS) and the samples' surface was characterized by Scanning Electron Microscopy (SEM) and Energy Dispersive Spectroscopy (EDS).

EXPERIMENTAL

Materials and media

The studied steel is AISI309 austenitic stainless steel whose chemical composition, established by spark spectroscopy, is shown in Table. 1.

The observation by light microscopy of the Nikon ECLIPSE LV 100ND shows an austenitic structure with precipitates at grain boundaries (Fig.1). The diffracto g X recorded on a diffracto meter BRUKER D8, adjusted by Maud software (Fig.2), identifies the following phases: an austenitic phase Feγ at 86% and the rest of $M_{23}C_6$ and M_7C_3 carbides.
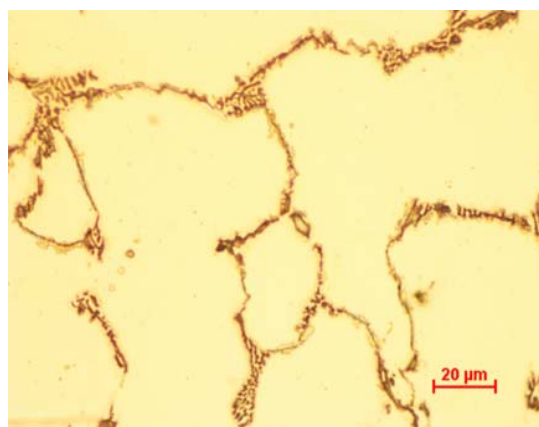
Fig. 1. Optical micrograph of AISI309 steel
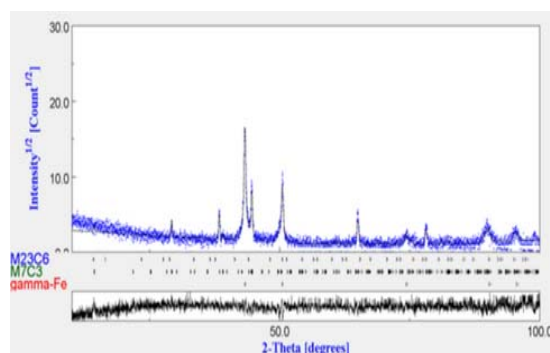
Fig. 2. Diffractogram of AISI309 steel

The experimental inhibitor is 2, 2'-Bipyridyl, supplied by the company Sigma-Aldrich and whose chemical structure is shown in Fig.3. The studied medium is 0.5 M H_2SO_4 without and with the concentrations 10^{-6}, 10^{-5}, and 10^{-4}M of 2,2'-Bipyridyl.

Gravimetric study

The gravimetric measurements were carried out on samples with the dimensions 1.2 cm x 1.35 cm x 0.7 cm in 50 ml of 0.5M H_2SO_4 without

Table .1: Chemical composition of AISI309 austenitic stainless steel (wt. %)

C	Si	Mn	P	S	Al	Cr	Ni	V
0.4	1.58	0.74	0.019	0.012	0.28	23.94	14.23	0.08

and with inhibitor's different concentrations. After 2 h immersion at 298 K, the samples were rinsed with distilled water and acetone and then dried and weighed using KERN ALS 220-4N analytical balance of precision ± 0.1 mg.
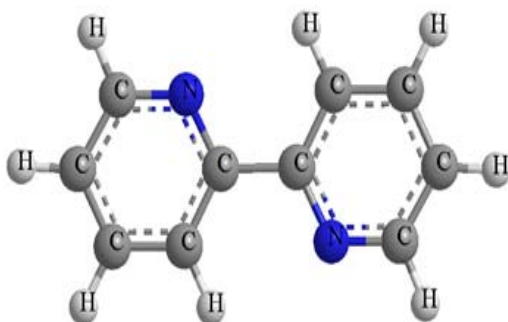
Fig. 3. Chemical structure of 2, 2'-Bipyridyl

Electrochemical measurements

Electrochemical measurements were carried out using Gamry interface 1000 potentiostat/galvanostat, associated with Gamry Framwork software and equipped with a conventional electrochemical cell with three electrodes: saturated calomel electrode (SCE), platinum counter electrode and AISI309 austenitic stainless steel working electrode. The latter is embedded in an epoxy resin delimiting 1cm² flat working surface, polished successively with silicon carbide (SiC) abrasive papers with different particle sizes: 600, 800, 1000 and 1200 and finally with 3μ diamond paste. After wards, it is washed with distilled water, degreased with acetone, then washed again with distilled water and finally dried under a dry air stream.

The electrochemical measurements were made after one hour immersion at 298 K: (a) the polarization curves (Tafel) are plotted by scanning the potential range (-600 to +970) mV vs. SCE at 1mV s^{-1} rate; (b) polarization resistance (R_p) was measured from the obtained polarization curves at ±10 mV relative to corrosion potential; and (c) electrochemical impedance spectroscopy's measurements (EIS) were carried out in the frequency range from 100 kHz to 10 mHz with 10 mV signal amplitude.

Surface analysis by MEB-EDS

The observation and analysis of samples surface were carried out, after 72 h immersion in 0.5M H_2SO_4 without and with 2,2'-Bipyridyl, by

Zeiss EVO MA25 scanning electron microscope, related to OXFORD X-Max^N energy dispersive spectroscopy (EDS)

RESULTS AND DISCUSSION

Mass loss measurement

Mass loss measurements of AISI309 stainless steel in 0.5M H_2SO_4 without and with different concentrations of 2,2'-Bipyridyl, after 2 hours immersion at 298K, were evaluated by the corrosion rate C_R and the inhibition efficiency $E_{WL}(\%)$, calculated by the following equations[24].

$$C_R = \Delta W / At \qquad (1)$$

Where:

ΔW: mass loss;

A: sample surface (cm²);

t: immersion time (h).

$$E_{WL}(\%) = [(C_{R0} - C_R) / C_{R0}] \times 100 \qquad (2)$$

Where C_{R0} and C_R are respectively the corrosion rates (mg cm^{-2} h^{-1}), without and with inhibitor addition in 0.5M H_2SO_4. The calculated values of corrosion rate (C_R) and inhibition efficiency (E_{WL} %) are shown in Table. 2.

Table. 2: Corrosion rate (C_R) Values and inhibition efficiency $E_{WL}(\%)$ obtained from gravimetric measurements

Concentration of inhibitor (M)	C_R (mg cm^{-2} h^{-1})	E_{WL} (%)
Blank	0.2150	-
10^{-6}	0.0745	65.34
10^{-5}	0.0575	73.25
10^{-4}	0.0358	83.34

The results (Table. 2) show that the inhibitor concentration's increase decreases the corrosion rate and consequently raises the inhibition efficiency which reaches 83.34% maximum value at 10^{-4}M (Fig.4). This increase is attributed to the adsorption of 2,2'-Bipyridyl molecules on steel surface leading to a protective film formation[25].

Measurements of electrochemical impedance spectroscopy

The electrochemical impedance spectra of AISI309 steel at 0.5M H_2SO_4 in Nyquist

representation, plotted after 1 h immersion without and with 2,2'-Bipyridyl, at the concentrations (10^{-6},10^{-5}et 10^{-4}M) are presented in Fig.5(a). Without 2,2'-Bipyridyl, the impedance spectrum is composed of two loops: a semicircular high frequency (HF) capacitive loop attributed to charge transfer reaction[26,27] and an inductive loop at low frequencies (LF) attributed either to relaxation process due to FeSO$_4$ species' adsorption or the inhibitor species on metal surface[28], and / or at passive film's re-dissolution[29]. With 2,2'-Bipyridyl, the impedance spectra are composed of a single capacitive loop indicating that the corrosion process is controlled by charge transfer phenomenon[11]. The inductive loop's disappearance with 2,2'-Bipyridyl addition results from the protective film formation on steel surface[30].
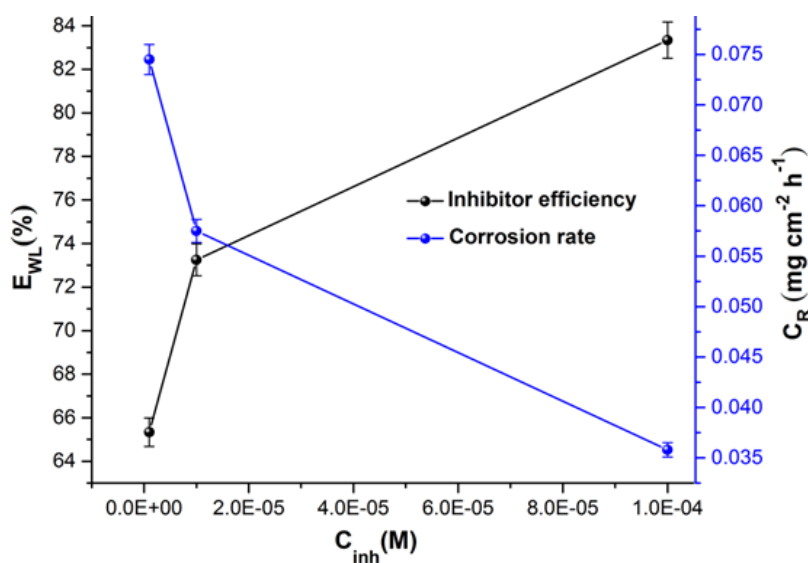
Fig. 4. Inhibition efficiency and corrosion rate according to the inhibitor concentration in 0.5 M H$_2$SO$_4$, obtained by the gravimetric method
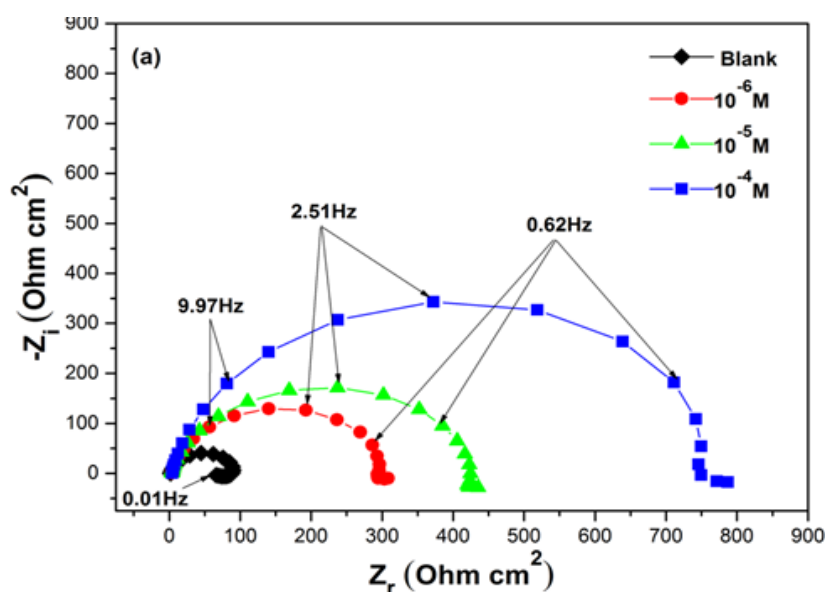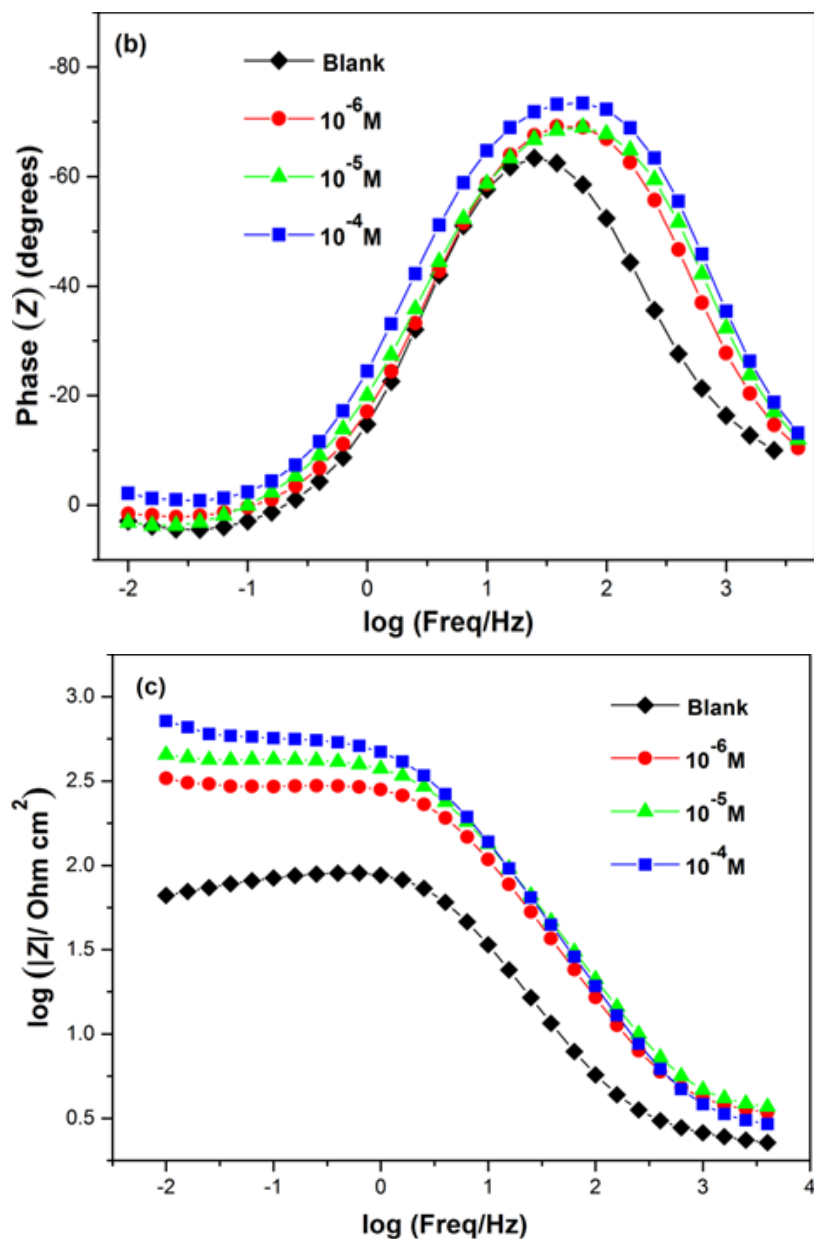
Fig. 5. Impedance diagrams of AISI309 steel in 0.5M H$_2$SO$_4$ at different concentrations of 2,2'-Bipyridyl in representation of Nyquist (a) and Bode according to the phase angle (b) and the modulus (c)

The Nyquist curves with 2,2'-Bipyridyl at different concentrations are wider than that without inhibitor, their diameters increase with the inhibitor concentration increasing, thereby improving the inhibition efficiency[31,32].

The obtained capacitive half-loops are not perfect; this may be attributed to the frequency dispersion effect, resulting from roughness and inhomogeneity of the electrode surface[33]. Therefore, instead of modeling the double layer by C$_{dl}$ capacitance, it is preferable to use a constant phase element (CPE) whose impedance is described by the expression[34].

$$Z_{CPE} = Q^{-1} (j \omega)^{-n} \qquad (3)$$

Where:

Q is the CPE constant;

ω is the angular frequency (in rad s^{-1});

$j^2 = -1$ is the imaginary number.

The exponent *n* can characterize different physical phenomena such as surface in homogeneities resulting from its roughness, inhibitor adsorption and porous layer's formation[35]; its values vary from 0 to -1 and characterize the CPE properties[36,37].

In Bode's representation, the phase angle Fig.5(b) increases with the inhibitor at different concentrations compared to that without 2,2'-Bipyridyl, this increase is due to inhibitor film's formation on metallic surface and ´|Z|´ modulus' increase Fig.5(c) indicates good inhibitor

performance[38]. The equivalent circuits deduced from the impedance curves in representation of Nyquist without and with inhibitor are shown respectively in Fig.6(a) and Fig.6(b).

Without inhibitor, the equivalent circuit is constituted of an electrolyte resistance (R_s), a constant phase element (CPE), a charge transfer resistance R_{ct}, an inductive resistance (R_L) and an inductance L. With inhibitor, the equivalent circuit is composed of an electrolyte resistance (R_s), a constant phase element (CPE) and a charge transfer resistance R_{ct}. From this electrical model, a parametric adjustment was made (Fig.7) showing that both experimental and simulated spectra are well correlated with an adequacy coefficient χ^2 of the order 23 x 10^{-3}.
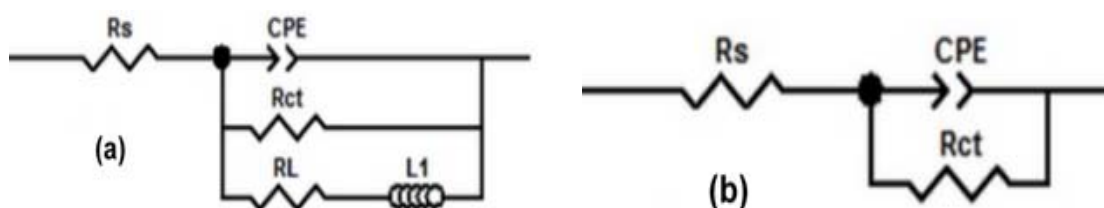
Fig. 6. Models of equivalent electrical circuits used for the impedances' analysis:
(a) without inhibitor, (b) with inhibitor
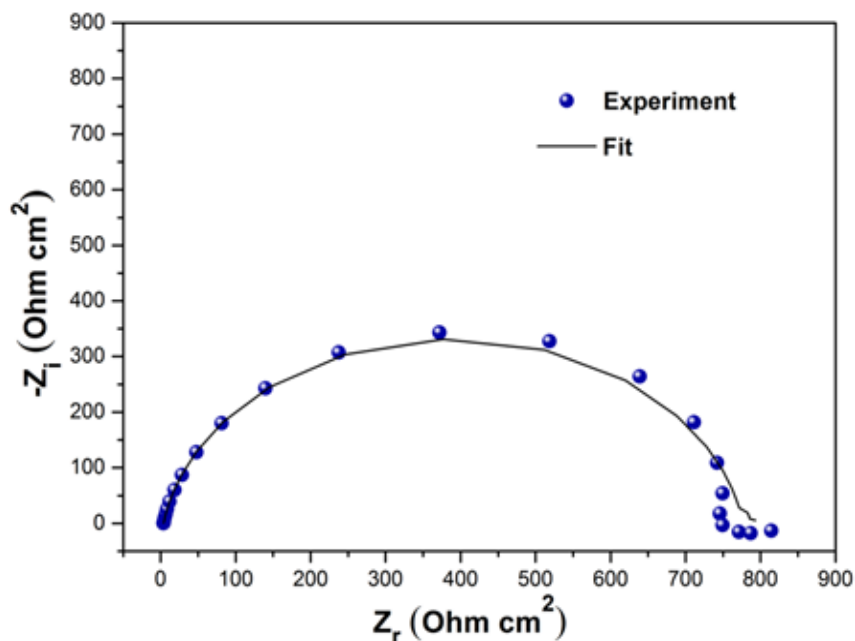
Fig. 7. Experimental and adjusted Nyquist's diagram of AISI309 steel in
0.5M H$_2$SO$_4$ containing 10^{-4}M 2,2'-bipyridyl

The values of various electrochemical parameters, deduced from the impedance spectra's parametric adjustment, are reported in Table 3. The corrosion's inhibition efficiencies are calculated from R_{ct} values according to the following equation[39]

$$E_{RT}(\%) = [(R_{ct} - R_{ct0}) / R_{ct}] \times 100 \qquad (4)$$

Where R_{ct0} and R_{ct} are respectively steel charge transfer resistances' values without and with inhibitor addition.

The values of these parameters show that: R_{ct} value rises with the inhibitor concentration increase; this is attributed to a protective film's formation at metal / solution interface, which enhances the inhibition efficiency[39]. The CPE values' reduction can result from the increase of the inhibitor film's thickness formed on metal surface may be due to 2,2'-bipyridyl molecules' adsorption at metal / solution interface[40].

The maximum R_{ct} (773Ω cm^2) and the minimum CPE (111. 5 µF cm^{-2}) are reached at the 10^{-4}M concentration of 2,2'-bipyridyl.

Table. 3: Electrochemical impedance parameters for AISI309 in 0.5M H$_2$SO$_4$ without and with addition of 2, 2'-bipyridyl various concentrations and the corresponding inhibition efficiency

Concentration of inhibitor (M)	R_s(Ω cm^2)	R_{ct}(Ω cm^2)	CPE(µF cm^{-2})	N	R_L(Ω cm^2)	L(H cm^2)	E_{Rt}(%)
Blank	2.17	94.39	749.4	0.868	289.2	551	-
10^{-6}	3.31	303.6	202.7	0.894	-	-	68.90
10^{-5}	3.42	424.8	179.4	0.875	-	-	77.78
10^{-4}	3.83	773	111. 5	0.902	-	-	87.78

The inhibition efficiency, calculated from Equation (4), rises according to 2,2'-bipyridyl's concentration's increase and reaches 87.78% maximum value at 10^{-4}M which is higher than that obtained by Ghazoui *et al*[19]., at 10^{-3}M imidazopyridine derivative.

Open circuit potential

Figure. 8 shows the variation of the AISI309 steel's open-circuit potential E_{OCP} without and with 10^{-4}M 2,2'-bipyridyl during 1 h of immersion without inhibitor, the open-circuit potential tends to stabilize at -395 mV / SCE, with inhibitor we note
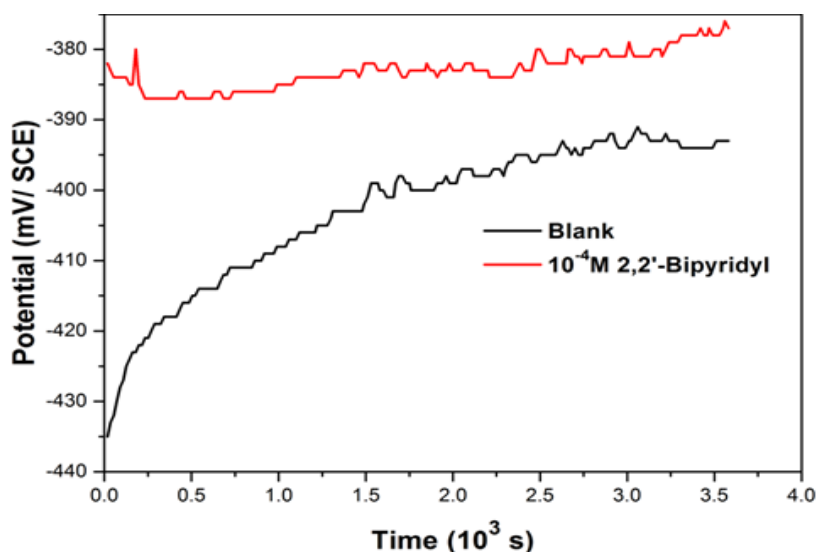
Fig. 8. Variation of the open-circuit potential according to time without and with10^{-4}M 2,2'-Bipyridyl

the E_{OCP} displacement towards more positive values which is due to the inhibitor's film formation.

Potentiodynamic (Tafel) polarization

Figure. 9 shows the samples' polarization curves (Tafel) in 0.5M H_2SO_4 without and with 2,2'-bipyridyl at different concentrations after 1 h of immersion at 298 K. The curves have the same general shape with an anodic passivation plateau in the potential range between -0.2 and +0.8 V vs. SCE. The inhibitor addition reduces the anodic and cathodic current's densities, shifts the corrosion potential to noble values and varies the Tafel's slope values. The βc change indicates 2,2'-bipyridyl influence on the cathodic reaction's kinetics. The variation of the βa anode branch's values may be due to the inhibitory molecules' adsorption on metal surface.
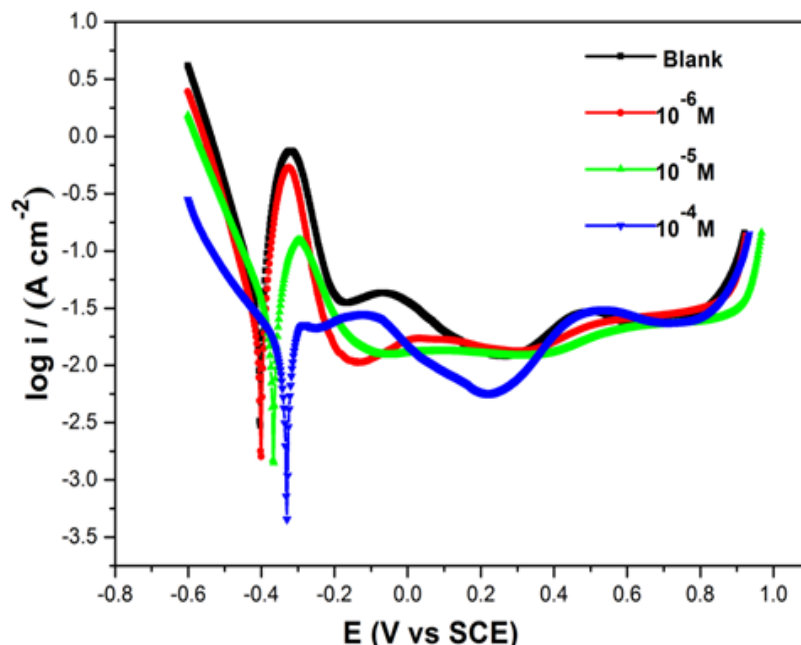
Fig. 9. Polarization curves (Tafel) of AISI309 steel in 0.5M H_2SO_4 containing different concentrations of 2,2'-bipyridyl

Generally, the inhibitor compound's classification depends on its influence on the shifting of the corrosion potential (d_{Ecorr}) compared to its value without inhibitor (E_{corr}). If d_{Ecorr} > 85 mV, the inhibitor is considered as an anodic or cathodic type, whereas if d_{Ecorr} < 85mV, it is considered to be a mixed type[25, 41]. In this study, d_{Ecorr} = +73 mV to the anodic direction indicating that the 2,2'-bipyridyl inhibitor acts as a mixed inhibitor with mainly an anodic effect. This behavior is due to 2,2'-bipyridyl molecules' adsorption which blocks the cathodic and anodic active sites by reducing the cathodic hydrogen release's rate and the slowing down of metal anodic dissolution's reactions[7].

In Table. 4, the electrochemical parameters are grouped, derived from the polarization curves (Tafel), such as the corrosion potential (E_{corr}), the slope of cathodic Tafel ($β_c$) and anodic ($β_a$), the corrosion current density (i_{corr}) and the polarization resistance (R_p) measured from the (LRP) method; Without inhibitor, i_{corr} = 55.57 µA cm^{-2} and R_p = 94.28 Ω cm^{-2}, they reach respectively 7.68 µA cm^{-2} and 753 Ω cm^{-2} at 10^{-4}M of 2,2'-bipyridyl.

The inhibition efficiencies E_i(%) and E_{Rp}(%) were calculated from the polarization resistance and the corrosion current density without and with inhibitor according to Eqs. (5) (6)[42].

$$E_i(\%) = [(i_{corr} - i_{corr(inhi)}) / i_{corr}] \times 100 \qquad (5)$$

Where:

i_{corr}: corrosion current density with inhibitor;

$i_{corr(inh)}$: corrosion current density without inhibitor.

$$E_{RP}(\%) = [(Rp_{(inh)} - Rp) / Rp_{(inh)}] \times 100 \qquad (6)$$

Where:

R_p: polarization resistance without inhibitor;
$R_{p(inh)}$: polarization resistance with inhibitor.

The best inhibition efficiency E_i (86.17%) obtained at 10^{-4}M 2,2'-bipyridyl is the same found by Bin Xu *et al.,*[16] at 3mM N-Bis (2-pyridylmethyl) aniline in 1 MHCl. We note a concordance of the obtained values E_i (86.17%) and E_{RP} (87.47%).

Adsorption Isotherm

In general, the molecules' adsorption process on metallic surface is reflected by water molecules' replacement adsorbed by organic molecules according to the following reaction[43].

$$Org_{(sol)} + xH_2O_{(ads)} \rightarrow Org_{(ads)} + xH_2O_{(sol)} \qquad (7)$$

Table. 4: Steel electrochemical parameters sat various concentrations of 2, 2'-bipyridyl in 0.5M H_2SO_4 and calculated inhibition efficiencies

Concentration of inhibitor (M)	E_{corr}(mV vs SCE)	i_{corr}(µA cm^{-2})	$-\beta c$(mV dec^{-1})	βa(mV dec^{-1})	Rp (Ω cm^2)	E_i(%)	E_{Rp}(%)
Blank	-403.7	55.57	104.7	56.4	94.28	-	-
10^{-6}	-401.4	17.83	86.0	37	325.3	67.91	71.01
10^{-5}	-366.9	14.89	83.7	52	467.4	73.20	79.82
10^{-4}	-330.6	7.68	124.8	79.4	753	86.17	87.47

Where:
$Org_{(sol)}$: dissolved organic molecules in solution;
$H_2O_{(sol)}$: water molecules in solution;
$Org_{(ads)}$: organic molecules adsorbed at metallic surface;
$H_2O_{(ads)}$: water molecules adsorbed at metallic surface;
x: water molecules' number substituted by organic molecules.

The adsorption mechanism as well as the inhibitors behavior can be explained by thermodynamic interpretation of the adsorption's isotherms, established from potentiodynamic polarization measurements.

The adsorption isotherm is represented by C_{inh}/θ graph according to C_{inhi} (Fig.10).

Where, the metallic surface coverage (θ) by the adsorbed atoms is calculated using the following equation [44].

$$\theta = E_i (\%) / 100 \qquad (8)$$

E_I (%): inhibition efficiency calculated depending on corrosion current densities.

The best adjustment gives a characteristic straight line of Langmuir isotherm whose regression coefficient's value (R^2 = 0.9998) is close to unity. According to this model, the surface coverage θ is linked to the adsorption equilibrium constant K_{ads} by the equation[41].

$$C_{inh} / \theta = 1/ K_{ads} + C_{inh} \qquad (9)$$

Where:
C_{inh} : inhibitor concentration;
K_{ads} can be calculated from the fit line's intersection on C_{inh} / θ axis.

The standard free energy of adsorption (ΔG^0_{ads}) is obtained according to the following equation[45]:

$$\Delta G = -RT \ln(55.5 K_{ads}) \qquad (10)$$
Where:
R: universal gas constant (8.314 J mol^{-1} K^{-1});
T: absolute temperature;

The value 55, 5 is the water concentration in solution (mol L^{-1}).

The high value of K_{ads} = 0.818 x 10^6 M^{-1} indicates 2,2'-Bipyridyl's strong adsorption on steel surface giving 86.17% à 10^{-4}M inhibition efficiency.

For $\Delta G_{ads} \leq$-20 kJ mol^{-1}, the organic molecules are physisorbed on metallic surface,

whereas for $\Delta G_{ads} \geq -40$ kJ mol^{-1}, the inhibitory molecules are chemisorbed on metallic surface by charge sharing or transfer[46]. In this study, the calculated value of ΔG_{ads} is -43.68 kJ mol^{-1}, thus 2,2'-bipyridyl adsorption is spontaneous and chemisorption.
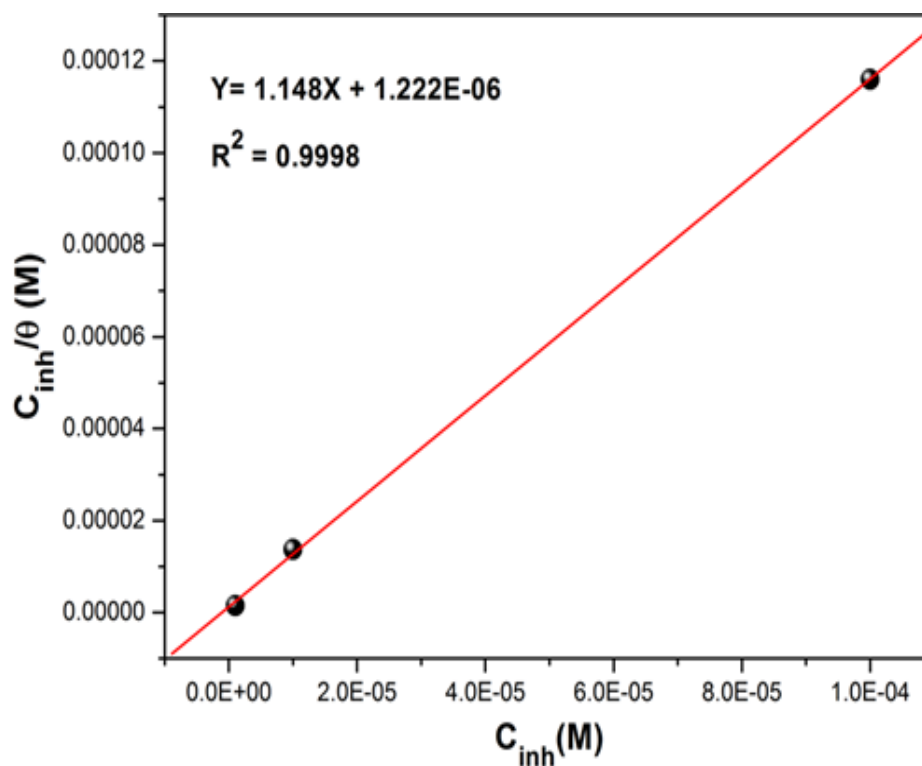
Fig. 10. Langmuir adsorption isotherm of AISI309 steel in 0.5M H$_2$SO$_4$ at 2,2'-Bipyridyl different concentrations

Scanning electron microscopy

Figure.11 shows samples surface's micrographs, obtained by MEB after 72 h of immersion in 0.5M H$_2$SO$_4$ without and with 2,2'-bipyridyl 10^{-4}M; without inhibitor (Fig. 11(a)), the surface is rough and strongly corroded; with inhibitor Fig. 11(b), it appears to be less attacked and has a rather smooth aspect; the spectra (EDS) corresponding to the 02 states are presented in Fig.12(a),(b). By comparison, the obtained elements' atomic percentages are reported in Table 5; the inhibited case demonstrates a peak's appearance at 4.09% nitrogen, a carbon percentage's increase from 9.46% to 20.25%, a decrease in iron percentage from 58.27% to 49.50% and the absence of sulfur peak. These results confirm the inhibitor molecules' adsorption on samples surface.

Table. 5: Elements' atomic percentages obtained from the EDS spectra

Media	Fe	Cr	C	O	S	N	Ni
0.5M H$_2$SO$_4$	58.27	17.44	9.46	4.41	0.89	0.00	9.54
0.5M H$_2$SO$_4$ +10^{-4} M 2,2'-bipyridyl	49.50	15.14	20.25	3.89	0.00	4.09	6.94
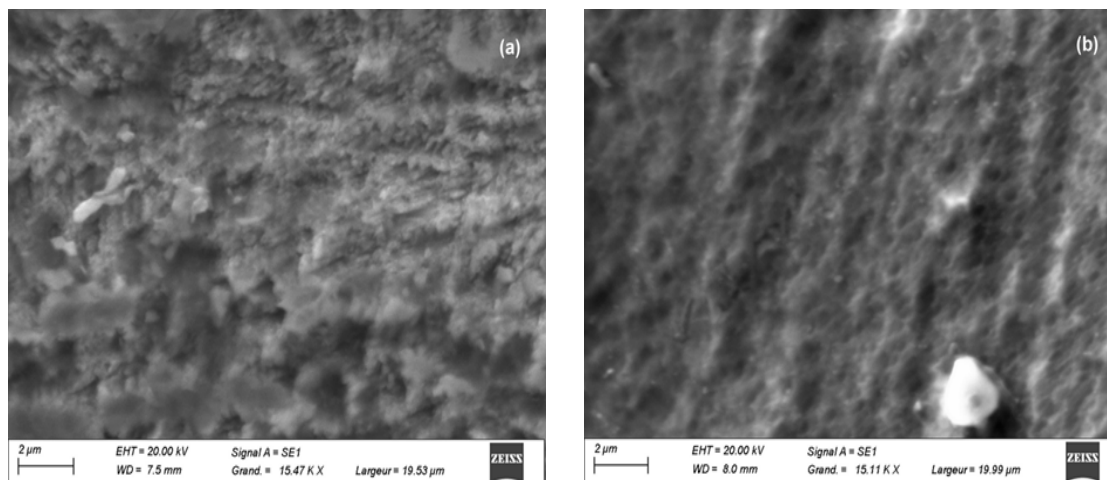
Fig.11. Steel MEB images after 72h immersion in 0.5M H_2SO_4, (a) without inhibitor, (b) with 10⁻⁴M 2,2'-bipyridyl
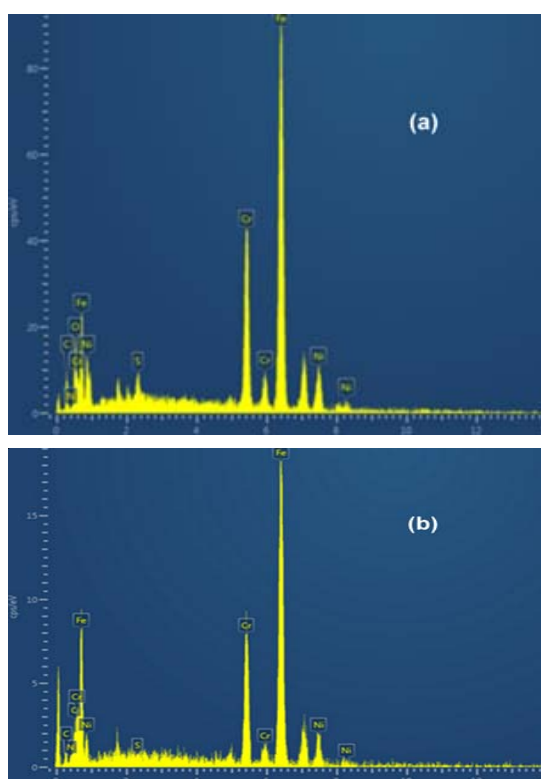
Fig. 12. Steel EDS spectra after 72h immersion in 0.5M H_2SO_4: (a) without inhibitor; (b) with 10⁻⁴M 2,2'-bipyridyl

CONCLUSION

The corrosion inhibition of AISI309 austenitic stainless steel by 2,2'-Bipyridyl in 0.5M H_2SO_4 was studied by gravimetric, potentiometric polarization (Tafel), electrochemical impedance spectroscopy, and micrographic analyzes by MEB and EDS. The obtained results show that:

1. 2,2'-bipyridyl presents good inhibitory properties, its efficiency is 83.34% at 10⁻⁴M.
2. 2,2'-bipyridyl acts as a mixed inhibitor with a mainly anodic effect.
3. The inhibitor concentration increase causes a raise of charge transfer resistance.
4. 2,2'-bipyridyl adsorption obeys to Langmuir isotherm and Gibbs energy ΔG_{ads} = -43.68 kJ mol⁻¹ indicates a lot more chemical than physical adsorption.
5. SEM observation and EDS analysis confirm an inhibitor film's formation on metallic surface.

REFERENCES

1. Pandya, S.; Ramakrishna, K.S.; Annamalai,A. R.; Upadhyaya, A. *Mater. Sci. Eng. A* **2012**, *556*, 271-277

2. BAI, G.; Lu, S.; Li, D.; Li, Y. *Corros. Sci.* **2016**, *108*, 111-124

3. Ibrahim, M. A. M.; Abd El Rehim, S. S; Hamza,

M. M. *Mater. Chem. Phys.* **2009**, *115*, 80-85

4. Mehdipour, M.; Naderi, R.; Markhali, B. P. *Prog. Org. Coat.* **2014**, *77*, 1761-1767

5. Yadav, M.; Kumar, S.; Purkait, T.; Olasunkanmi, L.O.; Bahadur, I.; Ebenso, E.E. *J. Mol. Liq.* **2016**, *213*, 122-138

6. Verma, C.; Ebenso, E.E.; Bahadur, I.; Obot, I.B.; Quraishi, M. A. *J. Mol. Liq.* **2015**, *212*, 209-218

7. Keles, H.; Keles, M. *Res. Chem. Intermed.* **2014**, *40*, 193-209

8. Karthik, G.; Sundaravadivelu, M.; Rajkumar, P. *Res. Chem. Intermed.* **2015**, *41*, 1543-1558

9. Gobara, M.; Baraka, A.; Zaghloul, B. *Res. Chem. Intermed.* **2015**, *41*, 7245-7261

10. Kosari, A.; Moayed, M.H.; Davoodi, A.; Parvizi, R.; Momeni, M.; Eshghi, H.; Moradi, H. *Corros. Sci.* **2014**, *78*, 138-150

11. John, S.; Jeevana, R.; Aravindakshan, K.K.; Joseph, A. *Egypt. J. Pet.* **2016**

12. Yadav, M.; Gope, L.; Sarkar, T.K. *Res. Chem. Intermed.* **2016,** *42*, 2641-2660

13. Ansari, K.R.; Quraishi, M.A.; Singh, A. *Meas.* **2015**, *76*, 136-147

14. Yüce, A.O; Telli, E.; Mert, B.D.; Kardaº, G.; Yazýcý, B. *J. Mol. Liq.* **2016,** *218*, 384-392

15. Yýldýz, R. ; Döner, A. ; Doðan, Dehri, T. Ý. *Corros. Sci.* **2014**, *82*, 125-132

16. Xu, B.; Ji, Y.; Zhang, X.; Jin, X.; Yang, W.; Chen, Y. *J. Taiwan Inst. Chem. Eng.* **2016**, *59*, 526-535

17. Sayin, K.; Jafari, H.; Mohsenifar, F. *J. Taiwan Inst. Chem. Eng.* **2016**, *68*, 431-439

18. Belkaid, S.; Tebbji, K.; Mansri, A.; Chetouani, A. ; Hammouti, B. *Res. Chem. Intermed.* **2012**, *38*, 2309-2325

19. Ghazoui, A.; Saddik, R.; Hammouti, B.; Zarrouk, A.; Benchat, N.; Guenbour, M.; Al-Deyab, S.S.; I. Warad, *Res. Chem. Intermed.* **2013**, *39*, 2369-2377

20. Karthik, R.; Vimaladevi, G.; Chen, S.M.; Elangovan, A.; Jeyaprabha, B.; P. Prakash, *Int. J. Electrochem. Sci.* **2015**, *10*, 4666-4681

21. Ansari, K.R.; Quraishi, M.A.; Singh, A. *J. Ind. Eng. Chem.* **2015,** *25*, 89-98

22. Hamza, M.M.; Abd El Rehim, S.S.; Ibrahim, M. A. M. *Arab. J. Chem.* **2013**, *6*, 413-422

23. Obaid, A.Y.; Ganash, A. A.; Qusti, A.H.; Elroby, S.A.; Hermas, A. A. *Arab. J. Chem.* **2013**

24. Amoozadeh, S. M.; Mahdavian, M.; *J. Mater. Eng. Perform.* **2015**, *24*, 2464-2472

25. El Faydy, M.; Galai, M.; El Assyry, A.; Tazouti, A.; Touir, R.; Lakhrissi, B.; Ebn Touhami, M.; Zarrouk, A. *J. Mol. Liq.* **2016**, *219*, 396-404

26. Jina, Z.H.; Gea, H.H.; Lina, W.W.; Zongb, Y.W.; Liub, S.J.; Shi, J.M. *Appl. Surf. Sci.* **2014**, *322*, 47-56

27. Sin, H. L.Y.; Umeda, M.; Shironita, S.; Abdul Rahim, A.; Saad, B. *Res. Chem. Intermed.* **2016**, 1-16

28. Abd El-Lateef, H. M. *Res. Chem. Intermed.* **2016**, *42*, 3219-3240

29. Khadiri, A.; Saddik, R.; Bekkouche, K.; Aouniti, Hammouti, A. B.; Benchat, N.; Bouachrine, M.; Solmaz, R. *J. Taiwan Inst. Chem. Eng.* **2016**, *58*, 552-564

30. Solmaz, R.; ºahin, E. A.; Doner, A.; Kardaª, G.; *Corros. Sci.* **2011**, *53*, 3231-3240

31. Lebrini, M.; Bentiss, F.; Chihib, N. E.; Jama, C.; Hornez, J. P.; Lagrenée, M. *Corros. Sci.*, **2008**, *50*, 2914-2918

32. Prabakaran, M.; Kim, S.H.; Hemapriya, V.; Chung, I. M. *Res. Chem. Intermed.*, **2016**, *42*, 3703-3719.

33. Lebrini, M.; Lagrenée, M.; Vezin, H.; Traisnel, M.; Bentiss, F. *Corros. Sci.*, **2007**, *49*, 2254-2269

34. Jiang, B.; Jiang, S.L.; Liu, X.; Ma, A.L.; Zheng, Y.G. *J. Mater. Eng. Perform.* **2015**, *24*, 4797-4808

35. Shabani-Nooshabadi, M.; Ghandchi, M.S. *J. Ind. Eng. Chem.* **2015**, *31*, 231-237

36. RameshKumar, S.; Danaee, I.; RashvandAvei, M.; Vijayan, M. *J. Mol. Liq.* **2015**, *212*, 168-186

37. Yilmaz, N.; Fitoz, A.; Ergun, Ü.; Emregül, K.C. *Corros. Sci.* **2016**, *111*, 110-120

38. Pavithra, M. K.; Venkatesha, T. V.; Punith Kumar, M. K.; Anantha, N. S. *Res. Chem. Intermed.* **2016**, *42*, 2409-2428

39. Raja, P.B.; Rahim, A.A.; Osman, H.; Awang, K. *Int. J. Miner. Metall. Mater.* **2011**, *18*, 413-418

40. Obot, I. B.; Madhankumar, A. *Mater. Chem. Phys.* **2016**, *177*, 266-275

41. Kumari, P.; Shetty, P.; Rao, S. A.; Sunil, D. *Trans. Indian. Inst. Met.* **2016**.

42. Anbarasi, K. Electrochemical and Corrosion Inhibition Studies of Cucurbita Maxima. *Orient. J. Chem.*, **2016***, 32*, 2139-2145.

43. Saranya, J.; Sounthari, P.; Kiruthika, A.; Saranya, G.; Yuvarani, S.; Parameswari, K.; Chitra, S. Experimental and quantum chemical studies on the inhibition potential of some quinoxaline derivatives for mild steel in acid media. *Orient. J. Chem,* **2014**, *30*, 1719-1736.

44. Baskar, R.; Gopiraman, M.; Kesavan, D.; Subramanian, K.; Gopalakrishnan, S. *J. Mater. Eng. Perform.* **2015**, *24*, 2847-2856

45. Sasikala, T.; Parameswari, K.; Chitra, S.; Synthesis and Corrosion Inhibition Study of Benzothiazepine Derivatives on Mild Steel in Acid Medium. *Orient. J. Chem.* **2016**, *32,* 1215-1222.

46. Liu, X.; Okafor, P. C.; Jiang, B.; Hu, H.; Zheng, Y. *J. Mater. Eng. Perform.* **2015**, *24,* 3599-3606